

Theory of active particle penetration through a planar elastic membrane

Abdallah Daddi-Moussa-Ider,^{1, a)} Benno Liebchen,^{1, 2} Andreas M. Menzel,¹ and Hartmut Löwen^{1, b)}

¹⁾*Institut für Theoretische Physik II: Weiche Materie, Heinrich-Heine-Universität Düsseldorf, Universitätsstraße 1, 40225 Düsseldorf, Germany*

²⁾*Theorie Weicher Materie, Fachbereich Physik, Technische Universität Darmstadt, Hochschulstraße 12, 64289 Darmstadt, Germany*

(Dated: May 24, 2022)

With the rapid advent of biomedical and biotechnological innovations, a deep understanding of the nature of interaction between nanomaterials and cell membranes, tissues, and organs, has become increasingly important. Active penetration of nanoparticles through cell membranes is a fascinating phenomenon that may have important implications in various biomedical and clinical applications. Using a fully analytical theory supplemented by particle-based computer simulations, the penetration process of an active particle through a planar two-dimensional elastic membrane is studied. The membrane is modeled as a self-assembled sheet of dipolar particles, uniformly arranged on a square lattice. A coarse-grained model is introduced to describe the mutual interactions between the membrane particles. The active penetrating particle is assumed to interact sterically with the membrane particles. State diagrams are presented to fully characterize the system behavior as functions of the relevant control parameters governing the transition between different dynamical states. Three distinct scenarios are identified. These comprise trapping of the active particle, penetration through the membrane with subsequent self-healing, in addition to penetration with permanent disruption of the membrane. The latter scenario is accompanied by a partial fragmentation of the membrane and creation of a hole of a size exceeding the interaction range of the membrane components. It is further demonstrated that the capability of penetration is strongly influenced by the size of the approaching particle relative to that of the membrane particles. Accordingly, active particles with larger size are more likely to remain trapped at the membrane for the same propulsion speed. Such behavior is in line with experimental observations. Our analytical theory is based on a combination of a perturbative expansion technique and a discrete-to-continuum formulation. It well describes the system behavior in the small-deformation regime. Particularly, the theory allows to determine of the membrane displacement and orientation fields of the dipolar particles in the trapping state. Our approach might be helpful for the prediction of the transition threshold between the trapping and penetration in real-space experiments involving motile swimming bacteria or artificial active particles.

I. INTRODUCTION

As one of the most fundamental components in biological systems, the cell membrane defines and protects the cell and is selectively permeable for ions and organic molecules, allowing to control the movement of required chemicals into the cell and of unwanted products out of the cell. It is now possible not only to reassemble cell membranes artificially¹, but also to design synthetic membranes with properties tailored to the needs of 21st centuries societies^{2–4}. In fact, synthetic membranes are now routinely used already for applications from water purification^{5, 6} to dialysis^{7, 8} and can be regarded as a paradigmatic success of biomimetics^{9–11}. Future perspectives for the usage of synthetic membranes involve problems like targeted gene and drug delivery to (cancer) cells^{12–22} or, more generally, the delivery of cargo to the interior of synthetic droplets, requiring a precise understanding of the interaction of motile particles with synthetic and biological membranes. Evidence from previous studies has shown that the physical uptake by living cells is strongly affected by the particle and membrane physicochemical and functional properties^{23–29}.

While membranes comprising active inclusions, e.g. in

the form of embedded proteins creating a stress on the membrane, have been studied for decades^{30–32}, the penetration of active particles through the membrane is less explored^{14, 33} with the few existing studies focusing on nano- and biotechnology perspectives. In particular, penetration of nanoparticles through a membrane has been studied using dissipative particle dynamics simulations, focusing on effects of particle shape¹⁴ and surface-structure³⁴. In addition, molecular dynamics simulations have been employed to investigate the penetration of fullerenes through lipid membranes³⁵. Recent studies have also explored interactions of active particles with membranes, from a more physical point of view, but did not focus on particle penetration^{36–38}. For a 1D membrane, we have recently performed a corresponding investigation³⁹.

Conversely to most of the above works, here we explore the penetration of an active particle through a 2D synthetic membrane from a physics perspective, aiming at predicting overall properties such as the membrane shape or the parameter domain leading to penetration starting from coarse microscopic details. We focus on a minimal model membrane that can be realized in principle using magnetic microparticles which are popularly employed as building blocks to self-assemble chains and sheets^{40–52}. To predict the state diagram, informing us about the parameter domains where particles can penetrate through the membrane and where they cannot, we systematically de-

^{a)}Electronic mail: abdallah.daddi.moussa.ider@uni-duesseldorf.de

^{b)}Electronic mail: hartmut.loewen@uni-duesseldorf.de

rive a continuum description of the membrane. We compare our results with particle-based computer simulations, finding close quantitative agreement regarding the transition between trapping and penetrating states, membrane shape and dynamics. Our analytical closed-form expressions might help to predict the properties of synthetic membranes, e.g. regarding the speed and size of particles which will be able to penetrate through them.

Below, we first define our model (Sec. II), followed by a brief discussion of the relevant parameters and of the 2D membrane dynamics as induced by the active particle approaching it (Sec. III). Here, besides a trapping state in which the membrane is deformed in the final state and does not allow the particle to pass, we find two scenarios of penetration. The first of these corresponds to the particle breaking through the membrane, followed by a complete self-healing of the membrane, which might be the desired behavior when delivering cargo towards a synthetic droplet or a healthy cell. The second scenario of penetration occurs mainly for larger particles, creating a hole in the membrane with a size exceeding the interaction range of the membrane components. This situation is accompanied by a partial fragmentation of the membrane structure into isolated particles. Following this qualitative discussion, we systematically explore the corresponding state diagram using numerical simulations, showing for which parameter combinations which of these three states prevails, and we develop a detailed analytical theory (Sec. IV). The latter is able to predict essentially the entire state diagram as well as the shape and the dynamics of the membrane, in close quantitative agreement with our simulations. Interestingly, the transition between self-healing and non-healing states is sharp, suggesting that there is a critical size for particles that pass a membrane by causing significant damage. This also suggests that if one were to permanently damage the membrane in our minimal model (and perhaps similarly in practice to treat cancer cells), one needs to use particles with a certain minimal size. Finally, concluding remarks summarizing our findings are contained in Sec. V.

II. SYSTEM SETUP

We examine the penetration mechanism of a non-fluctuating membrane by an active particle moving under the action of a constant propulsion force \mathbf{F}_0 . In this context, the penetrating particle may be viewed as a self-propelling agent in the limit of its persistence length being large compared to the distance initially separating the particle from the membrane^{53–64}. The active particle may represent a swimming microorganism^{65–70} or an artificial microrobot that can be manipulated by controlled external fields^{71–74}.

In our model, the membrane is composed of N identical dipolar spheres of radius a and dipole moment \mathbf{m} , uniformly arranged on a square lattice of size $L \times L$, rotated by 45° around the axis z , the latter directed normal to the membrane, as schematically illustrated in Fig. 1. We denote by h the lattice spacing after initialization. The dipole

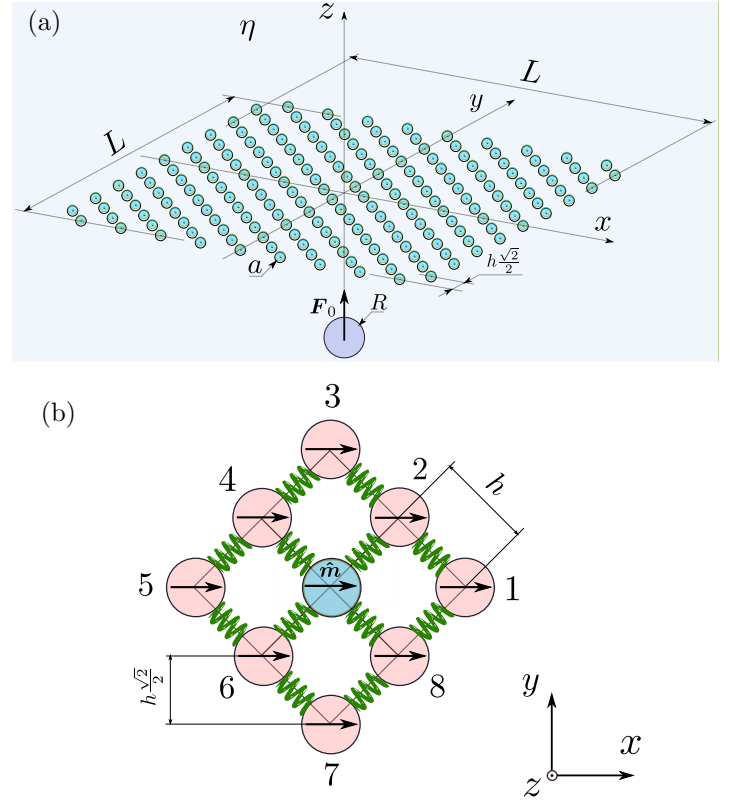


Figure 1. (Color online) Graphical illustration of the system setup. (a) An active particle of radius R moving through an effective driving force \mathbf{F}_0 toward a two-dimensional membrane composed of N dipolar particles of radius a and dipole moment \mathbf{m} . The membrane particles are initially arranged on a square lattice of dimension $L \times L$ and spacing h , rotated by 45° around the z axis, the latter oriented normal to the plane of the membrane. The membrane is centered about the origin and clamped at its periphery. Periodic boundary conditions are imposed in both x and y directions. We assume that the membrane particles are subject to dipolar, steric, and elastic pairwise interactions. The system is fully immersed in a Newtonian viscous fluid of shear viscosity η . (b) Schematic illustration of the lattice structure composing the model membrane. For future reference, the eight nearest neighbors of the particle at the center of the lattice are identified by numbers (1–8). Here, the dipoles are initially aligned along the x direction. Elastic springs are also inserted along the lattice diagonals but are not displayed here for reasons of clarity.

moments are rigidly attached to the particles and initially aligned along the x direction. The membrane is immersed in a Newtonian fluid, characterized by a constant dynamic viscosity η . We support the membrane at its periphery (the particle displacements are zero for $x, y = \pm L/2$) and assume periodic boundary conditions in the transverse directions (x, y). Moreover, we suppose that the mutual interactions between the membrane particles are pairwise additive and described by forces that depend only on the difference of coordinates of each two neighboring particles.

Typically, various types of interactions may occur among membrane particles including dipolar, steric, and elastic

interactions. For instance, dipolar and steric interactions can be imposed by membrane phospholipids chains and other biomolecules^{75–77}, whereas intermolecular coupling between the lipid bilayer and the cytoskeleton network gives rise to elastic interactions^{78–80}. Accordingly, the total potential energy of the membrane here is written as a sum of three distinct contributions as

$$\begin{aligned} \mathcal{U} = & \frac{\mu_0 m^2}{4\pi} \sum_{\substack{j=1 \\ j < i}}^N \frac{1}{r_{ij}^3} (\hat{\mathbf{m}}_i \cdot \hat{\mathbf{m}}_j - 3(\hat{\mathbf{m}}_i \cdot \hat{\mathbf{r}}_{ij})(\hat{\mathbf{m}}_j \cdot \hat{\mathbf{r}}_{ij})) \\ & + 4\epsilon \sum_{\substack{j=1 \\ j < i}}^N N_{ij} \left(\left(\frac{\sigma}{r_{ij}} \right)^6 \left(\left(\frac{\sigma}{r_{ij}} \right)^6 - 1 \right) + \frac{1}{4} \right) \\ & + \frac{k}{2} \sum_{i=1}^N \sum_{\substack{j \in \mathcal{N}(i) \\ j < i}} (r_{ij} - \xi r_{0ij})^2, \end{aligned} \quad (1)$$

wherein μ_0 is the vacuum permeability, while m represents the magnitude of the dipole moments which we assume to be constant and equal for the membrane particles. Moreover, $\hat{\mathbf{m}}_i = \mathbf{m}_i/m$ represents the unit orientation vector of the dipole moment \mathbf{m}_i of the i th particle, rigidly anchored to the particle frame. $r_{ij} = |\mathbf{r}_{ij}|$ is the distance between particles i and j , $\mathbf{r}_{ij} = \mathbf{r}_i - \mathbf{r}_j$, and $\hat{\mathbf{r}}_{ij} = \mathbf{r}_{ij}/r_{ij}$ is the corresponding unit distance vector. In addition, ϵ is an energy scale associated with the Weeks-Chandler-Anderson (WCA) pair-potential⁸¹, $\sigma = 2a$ is the diameter of the dipolar particles, $N_{ij} = H(r_C - r_{ij})$, with $H(\cdot)$ denoting the Heaviside step function, and $r_C = 2^{1/6}\sigma$ is a finite cutoff distance beyond which the steric interactions energy vanishes. Furthermore, k is the elastic constant of the harmonic springs coupling each particle to its four nearest and four next-nearest neighbors, r_{0ij} is the rest length of the springs, and $\xi \in (0, 1]$ is a prestress parameter. Here, we use the notation $\mathcal{N}(i)$ to denote the set of nearest and next-nearest neighbors of the i th membrane particle.

For the sake of simplicity, we neglect throughout this work all possible hydrodynamic interactions between particles. Moreover, we assume that the particles are small enough or sufficiently matched in density to the surrounding fluid for the influence of gravity to be neglected, and large enough for the effect of thermal fluctuations to be neglected.

The corresponding interaction force acting on the i th membrane particle is obtained by differentiating the potential energy described by Eq. (1) with respect to the particle position as $\mathbf{F}_i = -\partial\mathcal{U}/\partial\mathbf{r}_i$. Accordingly,

$$\begin{aligned} \mathbf{F}_i = & \frac{3\mu_0 m^2}{4\pi} \sum_{\substack{j=1 \\ j \neq i}}^N \frac{1}{r_{ij}^4} ((\hat{\mathbf{m}}_i \cdot \hat{\mathbf{r}}_{ij}) \hat{\mathbf{m}}_j + (\hat{\mathbf{m}}_j \cdot \hat{\mathbf{r}}_{ij}) \hat{\mathbf{m}}_i \\ & + (\hat{\mathbf{m}}_i \cdot \hat{\mathbf{m}}_j) \hat{\mathbf{r}}_{ij} - 5(\hat{\mathbf{m}}_i \cdot \hat{\mathbf{r}}_{ij})(\hat{\mathbf{m}}_j \cdot \hat{\mathbf{r}}_{ij}) \hat{\mathbf{r}}_{ij}) \\ & + 48\epsilon \sum_{\substack{j=1 \\ j \neq i}}^N \frac{N_{ij}}{r_{ij}} \left(\frac{\sigma}{r_{ij}} \right)^6 \left(\left(\frac{\sigma}{r_{ij}} \right)^6 - \frac{1}{2} \right) \hat{\mathbf{r}}_{ij} \end{aligned}$$

$$+ k \sum_{j \in \mathcal{N}(i)} (\xi r_{0ij} - r_{ij}) \hat{\mathbf{r}}_{ij}. \quad (2)$$

In addition, the resulting torque acting on the i th particle is of dipolar origin and can be calculated from the potential energy of the membrane as⁸² $\mathbf{T}_i = -\hat{\mathbf{m}}_i \times (\partial\mathcal{U}/\partial\hat{\mathbf{m}}_i)$. Defining the dimensionless vector $\mathbf{c}_{ij} = \hat{\mathbf{m}}_j - 3(\hat{\mathbf{m}}_j \cdot \hat{\mathbf{r}}_{ij}) \hat{\mathbf{r}}_{ij}$, we obtain

$$\mathbf{T}_i = -\frac{\mu_0 m^2}{4\pi} \sum_{\substack{j=1 \\ j \neq i}}^N \frac{\hat{\mathbf{m}}_i \times \mathbf{c}_{ij}}{r_{ij}^3}. \quad (3)$$

At small length scales, aqueous systems are characterized by small Reynolds numbers, so that viscous forces dominate over inertial forces. The resulting overdamped dynamics can therefore be adequately described within the framework of linear hydrodynamics^{83,84}. Accordingly, the translational and rotational velocities of the membrane particles, respectively denoted as \mathbf{V}_i and $\boldsymbol{\Omega}_i$, are linearly coupled to the forces and torques acting on their surfaces via the hydrodynamic mobility functions^{85–88}. The latter are second-order tensors, which simply reduce to scalar quantities when considering motion in an unbounded medium and neglecting the fluid-mediated hydrodynamic interactions between the particles. Specifically,

$$\mathbf{V}_i = \mu (\mathbf{F}_i + \mathbf{F}_i^{\text{ext}}), \quad (4a)$$

$$\boldsymbol{\Omega}_i = \gamma \mathbf{T}_i, \quad (4b)$$

where μ and γ denote, respectively, the translational and rotational self-mobility functions of the membrane particles. These are given by the usual Stokes formulas for an isolated sphere in an infinite fluid domain as $\mu = 1/(6\pi\eta a)$ and $\gamma = 1/(8\pi\eta a^3)$. In addition, $\mathbf{F}_i^{\text{ext}}$ represent the external force exerted by the active particle due to the steric interactions with the membrane particles. These pair interactions are modeled via a soft repulsive WCA potential as in Eq. (1) for which $\sigma = R + a$, with R denoting the radius of the active particle.

The equations governing the temporal evolution of the translational and rotational degrees of freedom of the i th membrane particle read

$$\frac{d\mathbf{r}_i}{dt} = \mathbf{V}_i, \quad (5a)$$

$$\frac{d\hat{\mathbf{m}}_i}{dt} = \boldsymbol{\Omega}_i \times \hat{\mathbf{m}}_i. \quad (5b)$$

The latter equation can further be reformulated after making use of Eqs. (3) and (4b) as

$$\frac{d\hat{\mathbf{m}}_i}{dt} = \frac{\gamma\mu_0 m^2}{4\pi} \sum_{\substack{j=1 \\ j \neq i}}^N \frac{1}{r_{ij}^3} ((\hat{\mathbf{m}}_i \cdot \mathbf{c}_{ij}) \hat{\mathbf{m}}_i - \mathbf{c}_{ij}). \quad (6)$$

We introduce at this point an additional cutoff length ℓ beyond which the dipolar and elastic interactions are set to zero. Accordingly, the dipolar and elastic potentials are

Dimensionless Number	Expression	Denomination
E_1	$\frac{\mu_0 m^2}{4\pi a^3 \epsilon}$	Reduced dipole strength
E_2	$\frac{a F_0}{\epsilon}$	Reduced activity
κ	$\frac{\pi k h^5}{6\mu_0 m^2}$	Reduced stiffness
δ	$\frac{R}{a}$	Size ratio
P_0	$\frac{1}{12} \left(\frac{h}{a}\right)^4 \frac{E_2}{E_1}$	Admittance

Table I. Expressions of essential dimensionless numbers that characterize the system in the trapping and penetrating states with the corresponding denominations.

also shifted to this cutoff length, so as to ensure that the resulting forces are continuous. Physically, ℓ may represent, for instance, an average distance between cytoskeleton-bilayer connection sites. Throughout this work, we set $\ell = 3h/2 > \sqrt{2}h$, such that the pair-interactions between the membrane particles are restricted to the four nearest and four next-nearest neighbors only.

III. TRAPPING, PENETRATION, AND SELF-HEALING

Having introduced a model for our membrane and derived the corresponding equations governing the translational and rotational dynamics of the particles composing the membrane, we next study in detail the dynamical states emerging from the interaction between an active particle propelling toward the membrane. For that purpose, we solve numerically the set of ordinary differential equations in time given by Eqs. (2) – (6) using a standard 4th-order Runge-Kutta scheme with adaptive time stepping⁸⁹. Before the active particle starts to interact with the membrane particles, we assume that the lattice spacing h is identical to the cutoff length scale r_C associated with the WCA pair potential. In addition, we assume that the rest length of the elastic springs is equal to the initial interparticle separation, i.e., $r_{0ij} = h$ for the pairs of particles located along the lattice axes, and $r_{0ij} = \sqrt{2}h$ for the pairs along the diagonal. Under these conditions, the membrane is initially at equilibrium, on account of the periodic boundary conditions imposed along the transverse directions (x, y). We further mention that requiring $h = r_C$ is equivalent to considering a constant ratio $h/a = 2^{7/6}$. Unless stated otherwise, we consider throughout the present article a membrane composed of $N = 450$ dipolar particles and set the prestress parameter as $\xi = 0.9$.

In analogy to our previous work on a 1D model membrane³⁹, we introduce four relevant dimensionless numbers that characterize the system behavior. We define the reduced dipole strength

$$E_1 = \frac{\mu_0 m^2}{4\pi a^3 \epsilon}, \quad (7)$$

which quantifies the importance of the dipolar forces ($\sim \mu_0 m^2/a^4$) relative to the steric forces ($\sim \epsilon/a$). Based on dimensional considerations, one might suppose that the membrane is endowed with an effective bending stiffness of the form $\kappa_B \propto E_1 \epsilon$, where the proportionality coefficient depends upon the membrane curvature and the number of particles constituting the membrane, as rigorously shown by Goriely and coworkers^{90,91}. In addition, we introduce the reduced activity

$$E_2 = \frac{a F_0}{\epsilon}, \quad (8)$$

which represents a balance between the magnitude of the active driving force F_0 and the steric forces. Further, we define the reduced stiffness

$$\kappa = \frac{\pi k h^5}{6\mu_0 m^2} \quad (9)$$

to represent the ratio between the elastic forces ($\sim ka$) and dipolar forces. Finally, we introduce the size ratio

$$\delta = \frac{R}{a} \quad (10)$$

to denote the radius of the active particle relative to that of the membrane particles.

An additional dimensionless parameter, that we denominate as “admittance”, is introduced to quantify the penetration capability of the active particle. It is defined based on the above definitions of E_1 and E_2 and expresses the ratio between active and dipolar forces. Specifically,

$$P_0 = \frac{1}{12} \left(\frac{h}{a}\right)^4 \frac{E_2}{E_1}. \quad (11)$$

The prefactor in front of the ratio E_2/E_1 follows from theoretical considerations as will be shown in the sequel. Here, the admittance serves to quantify a criterion of whether or not the active passes through the membrane. For ease of reference, the explicit expressions of the key dimensionless numbers characterizing the states of the system are listed in Tab. I.

To get a first intuition of the possible membrane dynamics, we display the different observed scenarios in Fig. 2. For low admittance ($P_0 \simeq 0.7$, top row and movie S1 in the Supporting Information), the membrane starts to deform when the motile active particle comes close, but only up to some point, reaching a steady state of constant membrane shape and fixed position of the active particle [see Fig. 2, panels (c) and (d)]. When increasing the admittance to $P_0 \simeq 2$ (second row and movie S2), the membrane

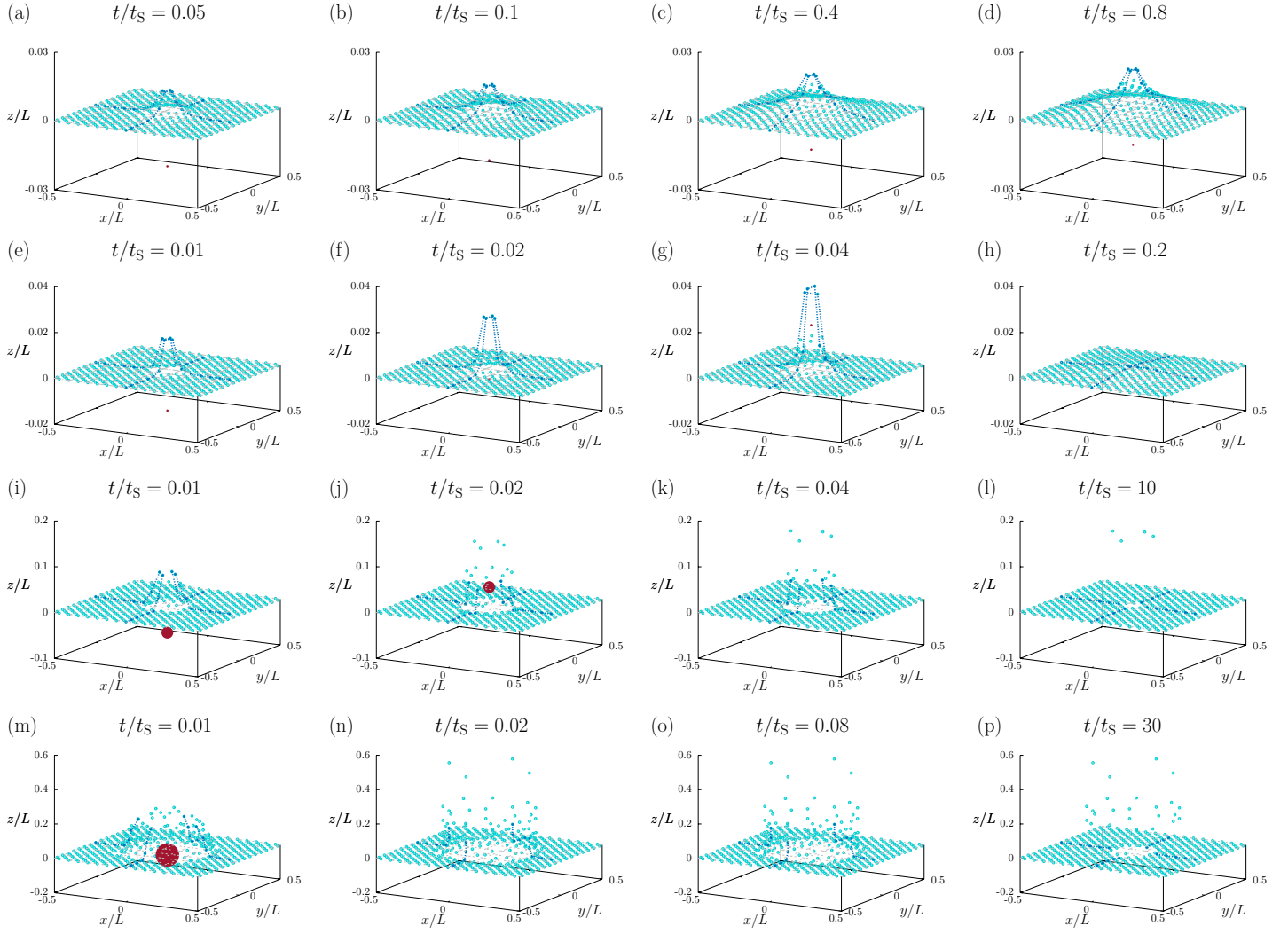


Figure 2. (Color online) Snapshots of particle-based computer simulations illustrating the membrane conformation in the trapping and penetration states at different time intervals scaled by the unit simulation time $t_S = \eta L^3 / \epsilon$. At time $t = 0$, the active particle begins interacting with the membrane particles (cyan circles). Here, we set the reduced stiffness $\kappa = 1$ in all these simulations. For clarity, the membrane particles located in the planes $x = 0$ and $y = 0$ within the interaction range of the dipolar and elastic potentials are shown as blue disks linked by dashed lines. The first row [panels (a) – (d)] displays the membrane dynamics in the trapping state, for a size ratio $\delta = 1$ and $(E_1, E_2) = (10^{-1}, 10^{-1.5})$. Since the driving force is not strong enough compared to the membrane restoring forces, the active particle remains trapped near the membrane. The second row [panels (e) – (h)] represents the time frames during penetration with subsequent self-healing, for $\delta = 1$ and $(E_1, E_2) = (10^{-1}, 10^{-1})$. In this state, the membrane recovers its initial planar shape after the active particle has passed through it. Next, the third row [panels (i) – (l)] contains the frame series during penetration without self-healing, for $\delta = 5$ and $(E_1, E_2) = (10^{-2}, 1)$. The membrane remains permanently damaged after penetration as the mutual distance between the four depicted fragmented particles becomes larger than the cutoff distance ℓ . The bottom row [panels (m) – (p)] further illustrates the penetration state without self-healing, for $\delta = 11$ and $(E_1, E_2) = (10^{-2}, 1)$. Due to the relatively large size of the active particle, the membrane is partially fragmented around its center into 24 isolated particles, the mutual distance between which is larger than the cutoff length ℓ . The red disks represent the positions of the active particle, which are out of the field of view in some panels. Because of the pronounced difference between the scales along the lateral and normal directions, the particles and their shapes are not plotted to scale.

no longer reaches a steady state, but the active particle breaks through the membrane, leaving a hole that starts to self-heal once the particle has left the membrane particles behind. Here, the membrane evolves back towards its original configuration, as it would be desired, e.g., when delivering cargo to the inside of a healthy cell, the membrane

of which we would want to remain intact. The membrane dynamics qualitatively changes when using larger particles instead ($\delta = 5$) and strongly enhancing the admittance to $P_0 \simeq 200$ (third row and movie S3). In this situation, the particle breaks through the membrane and creates a permanent hole. The four particles located around the center

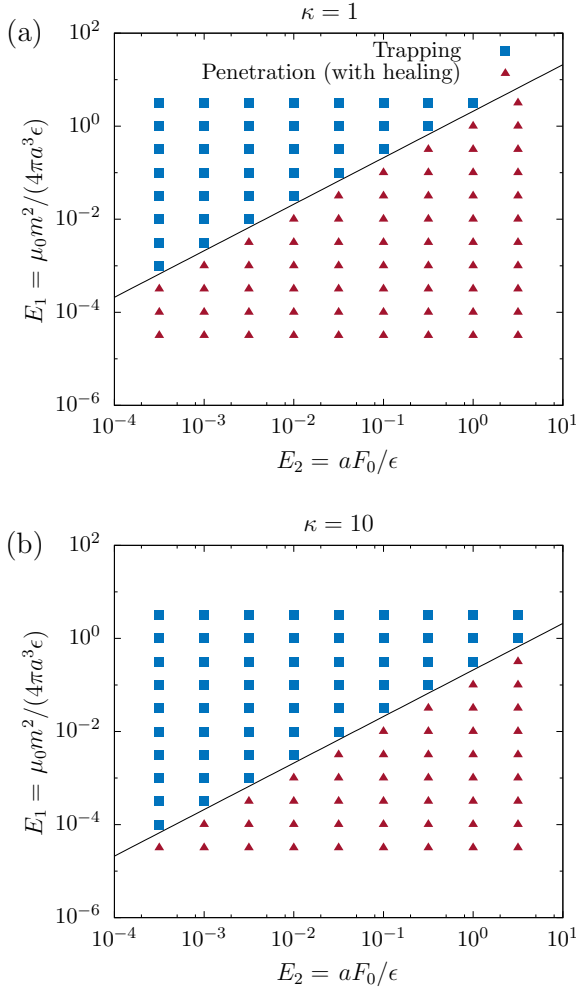


Figure 3. (Color online) State diagram of membrane penetration and trapping of an active particle in the parameter space (E_1, E_2) , for (a) $\kappa = 1$, and (b) $\kappa = 10$. Symbols correspond to the dynamical state resulting from numerically integrating the governing equations of motion stated by Eqs. (2) – (6). Here, we set the size ratio $\delta = 1$. The solid lines indicate an estimate of the transition between trapping (blue squares) and penetration (red triangles), given by $P_0 = \kappa$.

of the membrane in Fig. 2 (l) remain isolated because the range of the internal membrane interactions is shorter than the separation distance of these four particles from the rest of the membrane. Such a behavior is even more pronounced for significantly larger particles ($\delta = 11$) (bottom row and movie S4). In Fig. 2 (p), the membrane around the center is fragmented into 24 particles after the active particle has penetrated through the membrane.

In Fig. 3, we present state diagrams indicating the system behavior in the parameter space (E_1, E_2) for two different values of the reduced stiffness κ , namely, (a) $\kappa = 1$ and (b) $\kappa = 10$. As already mentioned, the membrane is composed of $N = 450$ dipolar particles. Here, we set $\delta = 1$. Depending on the ratio between the control parameters E_1 and E_2 , we observe that the active particle either passes

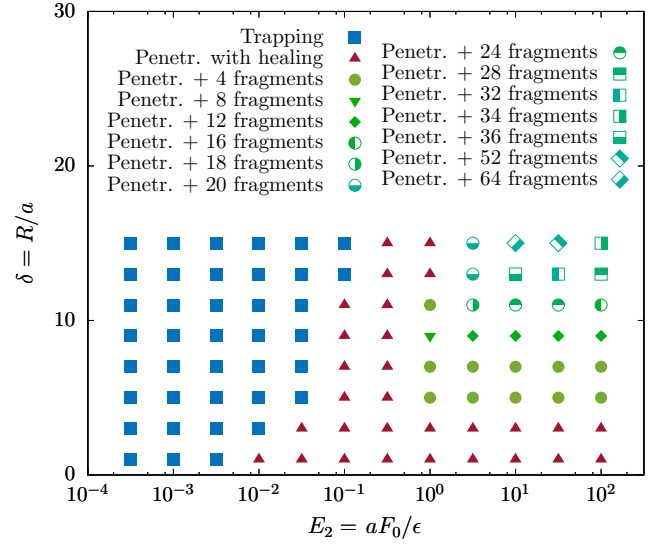


Figure 4. (Color online) State diagram in the parameter spaces (δ, E_2) for $E_1 = 10^{-2}$. We set the reduced stiffness $\kappa = 1$. Symbols represent the dynamical state resulting from numerical integration of the governing equations of motion given by Eqs. (2) – (6). In addition to trapping (blue squares) and penetration with healing (red triangles), penetration events without subsequent healing (green symbols) occur in some parameter ranges for large values of the size ratio δ . These penetration scenarios are accompanied by the creation of a permanent hole of a size exceeding the interaction range of the membrane particles in addition to the partial fragmentation of the membrane into isolated particles.

through the membrane to reach the other side (red triangles) or remains trapped (blue rectangles). The transition between the two states can be described by a linear hypothesis of the form $P_0 = \kappa$. Accordingly, penetration events occur when the membrane restoring forces consisting of dipolar and elastic contributions become weaker than the damaging force resulting from the steric interactions with the active particle. After full penetration has occurred, the membrane self-heals and relaxes back to its initial equilibrium configuration. We have systematically checked that an analogous state diagram holds for strongly elastic membranes as well, namely for $\kappa = 10^2$ and $\kappa = 10^3$.

In Fig. 4, we show dynamical state diagrams in the plane of the control parameters (δ, E_2) for $E_1 = 10^{-2}$. To limit the parameter space, we set the reduced stiffness to $\kappa = 1$. We observe that the transition between the trapping and penetration states can also be enabled by varying the aspect ratio δ . Accordingly, the penetration capability through a membrane is not only determined by the system admittance, but also by the size of the active particle relative to that of the membrane particles. This is in agreement with earlier experimental investigations indicating that particle size may strongly affect the uptake efficiency and kinetics^{92–96}. Consequently, an active particle with a size larger than that of the membrane particles is more likely to remain trapped. It is worth noting

that, in the considered range of parameters, the transition has been found to only depend on the admittance P_0 for our simplistic 1D model membrane studied in a previous work³⁹. For large values of the size ratio, the penetration process may also occur without subsequent self-healing of the membrane. This situation is accompanied by partial fragmentation of the membrane, during which a number of particles around the center remain isolated, creating a permanent hole in the membrane. The number of fragments largely depends on the propulsion speed and the size ratio. This effect points to an interesting size effect of the membrane behavior and shows that motile particles can be used to permanently damage the considered type of membrane.

IV. ANALYTICAL THEORY

To rationalize our numerical results, we derive in the following an analytical theory based on a perturbative expansion technique that describes the system behavior in the small-deformation regime. Particularly, we are interested to determine theoretically the membrane displacement and orientation fields of the dipolar particles in the trapping state. Our analytical calculations proceed through the linearization of the governing equations of motion, followed by prescribing the relevant fields using a discrete-to-continuum approach^{97,98}.

A. Linearized equations of motion

In the following, we neglect for simplicity the steric interactions between the membrane particles and assume that the mutual distance between neighboring particle is within the interaction range of the dipolar and elastic forces, i.e., $r_{ij} \in [h, \ell]$, with $j \in \mathcal{N}(i)$, for $i = 1, \dots, N$.

The dynamical equations governing the evolution of the i th membrane particle displacement and dipole orientation fields can be cast in the form

$$\dot{\mathbf{r}}_i = Ah^{-1} (\mathcal{F}_i^D + \mathcal{F}_i^E) + \mu \mathbf{F}_i^{\text{ext}}, \quad (12a)$$

$$\dot{\boldsymbol{\Omega}}_i = 2B \mathcal{T}_i, \quad (12b)$$

wherein the superposed dot represents a temporal deriva-

tive, and \mathcal{F}_i^D and \mathcal{F}_i^E are dimensionless forces stemming from the dipolar and elastic interactions, respectively. Here, we have defined for convenience the parameters

$$A = \frac{3\mu_0 m^2 \mu}{\pi h^3}, \quad B = \frac{3A}{8a^2}, \quad (13)$$

which have the dimension of a diffusion coefficient and inverse time, respectively.

Assuming that the active particle has a radius comparable to that of the membrane particles, i.e., for $\delta \sim 1$, it can readily be verified that the resistive force due to the steric interactions with the active particle vanishes only for the four particles located near the center of the membrane, the initial coordinates of which are given in the Cartesian coordinate system by $(x, y) = (\pm\sqrt{2}h/2, 0)$ and $(x, y) = (0, \pm\sqrt{2}h/2)$.

Adopting a local spherical coordinate system, the origin of which coincides with the center of the i th dipolar particle, the orientation vector can be represented as

$$\hat{\mathbf{m}}_i = \begin{pmatrix} \cos \psi_i \cos \phi_i \\ \cos \psi_i \sin \phi_i \\ \sin \psi_i \end{pmatrix}, \quad (14)$$

where $\phi_i \in [0, 2\pi)$ denotes the azimuthal angle, and $\psi_i = \pi/2 - \theta_i$ stands for the complement of the polar angle, with $\theta_i \in [0, \pi]$. In the initial configuration, $\phi_i = \psi_i = 0$, for $i = 1, \dots, N$. Accordingly, the rotation rate of the i th dipolar particle can be obtained using Euler representation as

$$\boldsymbol{\Omega}_i = \begin{pmatrix} \dot{\psi}_i \sin \phi_i \\ -\dot{\psi}_i \cos \phi_i \\ \dot{\phi}_i \end{pmatrix}. \quad (15)$$

Following a linear elasticity theory approach^{99,100}, we express the position vectors of each dipolar particle relative to the laboratory frame as $\mathbf{r}_i = (U_i + u_i) \hat{\mathbf{e}}_x + (V_i + v_i) \hat{\mathbf{e}}_y + w_i \hat{\mathbf{e}}_z$, for $i = 1, \dots, N$, where $U_i \hat{\mathbf{e}}_x + V_i \hat{\mathbf{e}}_y$ is the position vector in the undeformed state of reference, and $u_i \hat{\mathbf{e}}_x + v_i \hat{\mathbf{e}}_y + w_i \hat{\mathbf{e}}_z$ is the displacement of the membrane particles relative to the initial configuration. The linearized magnetic force acting on the i th dipolar particle reads

$$\mathcal{F}_i^D = \begin{pmatrix} \frac{\sqrt{2}}{4} (p_1 + p_5) - \frac{13}{16} S_p + \frac{3\sqrt{2}}{32} (p_3 + p_7) + \frac{5}{16} (q_2 - q_4 + q_6 - q_8) + \frac{3\sqrt{2}}{16} (\phi_2 + \phi_4 - \phi_6 - \phi_8) + \frac{1}{16} (\phi_7 - \phi_3) \\ \frac{5}{16} (p_2 - p_4 + p_6 - p_8) - \frac{\sqrt{2}}{8} Q_q + \frac{19}{16} S_q + \frac{1}{16} (\phi_5 - \phi_1) + \frac{3\sqrt{2}}{16} (\phi_2 - \phi_4 - \phi_6 + \phi_8) \\ - \frac{\sqrt{2}}{8} (r_1 + r_5) - \frac{3}{8} S_r + \frac{\sqrt{2}}{32} (r_3 + r_7) + \frac{1}{16} (\psi_5 - \psi_1) + \frac{\sqrt{2}}{8} (\psi_4 - \psi_2 + \psi_6 - \psi_8) \end{pmatrix}, \quad (16)$$

where we have defined $p_j = (u_j - u_i)/h$, $q_j = (v_j - v_i)/h$, and $r_j = (w_j - w_i)/h$ to denote the displacement gradients. Here, the numbers $j = 1, \dots, 8$ appearing in subscript denote the index of a nearest or next-neighbor particle on the lattice, as schematically illustrated in Fig. 1 (b). Moreover, we have used the shorthand notations $S_\alpha = \alpha_2 + \alpha_4 + \alpha_6 + \alpha_8$, $Q_\alpha = \alpha_1 + \alpha_3 + \alpha_5 + \alpha_7$, for $\alpha \in \{p, q, r, \psi, \phi\}$, in addition to $W = p_2 + p_4 - p_6 - p_8 + q_2 - q_4 - q_6 + q_8$.

Analogously, the elastic force acting on the i th particle can be presented in a linearized form as

$$\mathcal{F}_i^E = -\kappa \begin{pmatrix} 2(p_1 + p_5) + (2 - \xi)S_p + 2(1 - \xi)(p_3 + p_7) + \xi(q_2 - q_4 + q_6 - q_8) \\ \xi(p_2 - p_4 + p_6 - p_8) + 2(1 - \xi)(q_1 + q_5) + (2 - \xi)S_q + 2(q_3 + q_7) \\ 2(1 - \xi)(S_r + Q_r) \end{pmatrix}. \quad (17)$$

Notably, the inplane components of the dipolar and elastic forces involve gradients of the lateral displacements p_j and q_j in addition to the azimuthal orientation ϕ_j . In contrast to that, the normal components are found to depend on the displacement gradient r_j and the complement of the polar angle ψ . Consequently, a decoupling between the lateral and normal displacements is found for planar membranes, in a way analogous to what has previously been observed for 2D elastic membranes that are modeled as a continuum hyperelastic material featuring resistance toward shear and bending^{101–104}. Particularly, for a non-prestressed membrane ($\xi = 1$), the elastic forces are purely tangential (oriented along the plane of the membrane) and depend solely on the inplane displacement gradients p_j and q_j .

Finally, the linearized dipolar torque has components only along the y - and z -axes and can be expressed in terms of the displacement gradients and dipole orientation angles in a scaled form as

$$\mathcal{T}_i = \begin{pmatrix} 0 \\ \frac{1}{16}(r_1 - r_5) + \frac{\sqrt{2}}{8}(r_2 - r_4 - r_6 + r_8) + \left(\frac{1}{6} + \frac{\sqrt{2}}{24}\right)\psi_i + \frac{\sqrt{2}}{48}Q_\psi + \frac{1}{12}S_\psi \\ \frac{3\sqrt{2}}{16}W + \frac{1}{16}(p_7 - p_3 - q_1 + q_5) - \left(\frac{1}{6} + \frac{\sqrt{2}}{24}\right)\phi_i + \frac{\sqrt{2}}{48}(2\phi_3 - \phi_1 - \phi_5 + 2\phi_7) + \frac{1}{24}S_\phi \end{pmatrix}. \quad (18)$$

Having derived linearized expressions for the forces and torques governing the evolution of the membrane particles, we next consider the dynamics of the active particle. The latter is subject to the active driving force $\mathbf{F}_0 = F_0 \hat{\mathbf{e}}_z$ in addition to the repulsive steric forces resulting from the interaction with the nearby membrane particles. In the overdamped regime, the translational motion of the active particle along the z direction is governed by

$$6\pi\eta R \dot{z}_P = F_0 - 4F \cos \alpha, \quad (19)$$

wherein z_P denotes the z -position of the active particle, and F stands for the magnitude of the steric force exerted by one of the four particles located around the membrane center, and α denotes the angle this force makes with the vertical.

Equations (12) form $2N$ ordinary differential equations in the time variable for the unknown membrane displacement and dipole orientation fields. These equations are subject to the initial conditions of vanishing membrane displacement and reorientation angles of the dipoles, in addition to vanishing displacement at the membrane periphery and periodic boundary conditions along the x and y directions. In the steady state, the problem is equivalent to searching for the solution of linear recurrence relations coupling the positions and orientations of all the membrane particles initially located on a lattice. Due to the somewhat complicated nature of the resulting equations, an analytical solution is far from being trivial. To handle this difficulty and to obtain a quantitative insight into the system behavior in the small-deformation regime, we will approach the problem differently. Our solution methodology will be based on a continuum description of the linearized equa-

tions of motion as detailed below.

B. Continuum theory

The core idea of discrete-to-continuum analysis, is to express the membrane displacements and dipole orientations following the standard approach as

$$\begin{pmatrix} u_{i+s,i+r} \\ v_{i+s,i+r} \\ w_{i+s,i+r} \\ \phi_{i+s,i+r} \\ \psi_{i+s,i+r} \end{pmatrix} = \exp(h\sqrt{2}(sD_x + rD_y)) \begin{pmatrix} u(x,y) \\ v(x,y) \\ w(x,y) \\ \phi(x,y) \\ \psi(x,y) \end{pmatrix}, \quad (20)$$

where $D_\alpha = \partial/\partial\alpha$, $\alpha \in \{x, y\}$ represents the differential operator and $(s, r) \in \{0, \pm 1/2, \pm 1\}$. Here, the fraction at subscripts $i \pm 1/2$ refer to the nearest-neighboring particle on the lattice axes, namely, the ones identified by even numbers in Fig. 1 (b). The integer subscripts $i \pm 1$ refer to the next-nearest-neighboring particles located on the lattice diagonals.

The exponential argument in Eq. (20) can be expanded up to the second order in power series using a two-dimensional Taylor expansion as¹⁰⁵

$$\exp(h\sqrt{2}(sD_x + rD_y)) = 1 + h\sqrt{2}(sD_x + rD_y) + h^2(s^2D_x^2 + 2srD_xD_y + r^2D_y^2) + \dots \quad (21)$$

Applying this transformation rule to Eq. (12a), the partial differential equation governing the translational degrees of freedom of the membrane particles can be rewritten in vector form as

$$\frac{1}{A} \begin{pmatrix} u,t \\ v,t \\ w,t \end{pmatrix} = \begin{pmatrix} \left(\frac{13}{16} - \frac{\sqrt{2}}{2}\right) u,xx + \left(\frac{13}{16} - \frac{3\sqrt{2}}{16}\right) u,yy - \frac{5}{8} v,xy + \left(\frac{3}{4} - \frac{\sqrt{2}}{8}\right) \phi,y \\ -\frac{5}{8} u,xy + \left(\frac{\sqrt{2}}{4} - \frac{19}{16}\right) (v,xx + v,yy) + \left(\frac{3}{4} - \frac{\sqrt{2}}{8}\right) \phi,x \\ \left(\frac{3}{8} + \frac{\sqrt{2}}{4}\right) w,xx + \left(\frac{3}{8} - \frac{\sqrt{2}}{16}\right) w,yy - \left(\frac{1}{2} + \frac{\sqrt{2}}{8}\right) \psi,x \end{pmatrix} + \kappa \begin{pmatrix} (6-\xi) u,xx + (6-5\xi) u,yy + 2\xi v,xy \\ (6-5\xi) v,xx + (6-\xi) v,yy + 2\xi u,xy \\ 6(1-\xi) (w,xx + w,yy) \end{pmatrix} + \frac{h^2}{A} (\mu F_0 - \delta \dot{z}_P) \delta(x, y) \hat{e}_z, \quad (22)$$

where we have approximated the steric force exerted on the particles near the center of the membrane by a two-dimensional Dirac delta function $\delta(x, y) = \delta(x)\delta(y)$. We have checked that taking alternative forms for the steric force, such as a 2D rectangle function centered around the origin, does not alter our results significantly. Therefore, a Dirac delta function has been adopted here for simplicity. As for the rotational degree of freedom given by Eq. (12b), a discrete-to-continuum transformation yields

$$\frac{1}{B} \begin{pmatrix} \psi,t \sin \phi \\ -\psi,t \cos \phi \\ \phi,t \end{pmatrix} = \begin{pmatrix} 0 \\ \left(1 + \frac{\sqrt{2}}{4}\right) (\psi - w,x) \\ \left(\frac{\sqrt{2}}{4} - \frac{3}{2}\right) (u,y + v,x) \end{pmatrix}. \quad (23)$$

In the steady-state limit, it follows readily from Eq. (23) that $\psi - w,x = 0$ and $u,y + v,x = 0$. Accordingly, the steady polar orientation of the dipolar particles only depends on the displacement gradient. Interestingly, this situation is in analogy with the Kirchhoff–Love theory for elastic beams or sheets⁹⁹. Under these conditions, Eq. (22) for the translational degrees of freedom simplifies to

$$\begin{pmatrix} \left(\frac{13}{16} - \frac{\sqrt{2}}{2}\right) u,xx + \left(\frac{23}{16} - \frac{3\sqrt{2}}{16}\right) u,yy + \left(\frac{3}{4} - \frac{\sqrt{2}}{8}\right) \phi,y \\ \left(\frac{\sqrt{2}}{4} - \frac{9}{16}\right) v,xx + \left(\frac{\sqrt{2}}{4} - \frac{19}{16}\right) v,yy + \left(\frac{3}{4} - \frac{\sqrt{2}}{8}\right) \phi,x \\ \left(\frac{\sqrt{2}}{8} - \frac{1}{8}\right) w,xx + \left(\frac{3}{8} - \frac{\sqrt{2}}{16}\right) w,yy \end{pmatrix} + \kappa \begin{pmatrix} (6-\xi) u,xx + (6-7\xi) u,yy \\ (6-7\xi) v,xx + (6-\xi) v,yy \\ 6(1-\xi) (w,xx + w,yy) \end{pmatrix} + \begin{pmatrix} 0 \\ 0 \\ hP_0 \end{pmatrix} \delta(x, y) = \mathbf{0}, \quad (24)$$

wherein $P_0 = \mu h F_0 / A$, is the system admittance defined above by Eq. (11). We recall that $P_0 \sim E_2 / E_1$. In Eq. (24), we explicitly observe that P_0 controls how far the active particle can penetrate through the initial planar membrane and leads to a deflection of the membrane. We note that the 2D Dirac delta function has the dimension of inverse length squared. In the following, we attempt to obtain closed analytical expressions for the displacement and orientation fields not only for the steady state but also for transient dynamics situations.

C. Steady solution

Because of the already-mentioned decoupling between the lateral and normal displacements, the solution for the in- and out-of-plane deformations can be obtained independently. Since the external force is exerted normal to the plane of the membrane, deformation will predominantly occur along the z direction. In the following, we assume that $|w| \ll L$, for our approximate equations of motion derived above to be valid.

By projecting Eq. (24) onto the z direction, the normal displacement is governed by a second-order partial differential equation of the form

$$k_{\parallel} w,xx + k_{\perp} w,yy + hP_0 \delta(x, y) = 0, \quad (25)$$

where

$$k_{\parallel} = c - \frac{5}{8} + 6(1-\xi)\kappa, \quad (26a)$$

$$k_{\perp} = \frac{5}{8} - \frac{c}{2} + 6(1-\xi)\kappa, \quad (26b)$$

are dimensionless numbers that comprise both dipolar and elastic contributions. For future reference, we have defined the constant

$$c = \frac{1}{2} + \frac{\sqrt{2}}{8}. \quad (27)$$

By rescaling the spatial variables, $x = X\sqrt{k_{\parallel}}$ and $y = Y\sqrt{k_{\perp}}$, Eq. (25) can be presented in the form of a steady diffusion equation with a source term as

$$w,XX + w,YY + \frac{hP_0}{\sqrt{k_{\parallel}k_{\perp}}} \delta(X)\delta(Y) = 0. \quad (28)$$

As $k_{\parallel} < k_{\perp}$, the deformation profile is expected to be broader (high variance distribution) along the y direction than along the x direction, when considering weakly elastic membranes for which $\kappa \ll 1$. For strongly elastic membranes (with $\xi \neq 1$), it follows that $k_{\parallel} \simeq k_{\perp}$, and thus the system behavior is primarily determined by membrane elasticity and approximately isotropic.

To solve Eq. (25), we exploit periodicity of the system along the transverse directions by expressing the membrane normal displacement w in terms of a Fourier series¹⁰⁶. Then,

$$w(x, y) = \frac{4}{L^2} \sum_{p \geq 1} \sum_{q \geq 1} \hat{w}(p, q) c_p(x) c_q(y), \quad (29)$$

with $p, q = 1, 2, \dots$ denoting the positive integers that set the coordinates in Fourier space. Here, we have defined the basis function $c_p(x) = \cos(H_p x)$, where $H_p = (2p-1)\pi/L$, and analogously for $c_q(y)$. In addition, $\hat{w}(p, q)$ denotes the Fourier coefficients of w , defined as

$$\hat{w}(p, q) = \int_{-\frac{L}{2}}^{\frac{L}{2}} \int_{-\frac{L}{2}}^{\frac{L}{2}} w(x, y) c_p(x) c_q(y) dx dy. \quad (30)$$

It is worth mentioning that the solution form given by Eq. (29) follows from the prescribed boundary conditions, so as to ensure that $w(x = \pm L/2, y) = w(x, y = \pm L/2) = 0$. Moreover, the basis functions $c_p(x)$ satisfies the orthogonality relation

$$\int_{-\frac{L}{2}}^{\frac{L}{2}} c_p(x) c_{p'}(x) dx = \frac{L}{2} \delta_{pp'}. \quad (31)$$

By substituting Eq. (29) into Eq. (25) and making use of the orthogonality property given by Eq. (31), we readily obtain

$$\hat{w}(p, q) = \frac{hP_0}{k_{\parallel} H_p^2 + k_{\perp} H_q^2}. \quad (32)$$

For the torque balance equation, it follows from Eq. (23) that the steady orientation of the membrane dipoles is obtained as

$$\psi(x, y) = w_{,x} = -\frac{4}{L^2} \sum_{p \geq 1} \sum_{q \geq 1} H_p \hat{w}(p, q) s_p(x) c_q(y), \quad (33)$$

where we have defined the basis functions $s_p(x) = \sin(H_p x)$. Particularly, $\psi(x = 0, y) = 0$, as required by the symmetry of the system.

Finally, by writing the solution for the transverse displacements $u(x, y)$ and $v(x, y)$ in terms of Fourier series in a way analogous to Eq. (29) and the azimuthal orientation of the dipoles as

$$\phi(x, y) = \frac{4}{L^2} \sum_{p \geq 1} \sum_{q \geq 1} \hat{\phi}(p, q) s_p(x) s_q(y), \quad (34)$$

it follows that u, v , and ϕ must vanish to satisfy the boundary conditions imposed at the membrane extremities, considering the present approximate equations.

Figure 5 shows the steady-state variations of (a) the normal displacement (scaled by the membrane size) and (b) the dipole orientation angle ψ versus x/L . Results are shown in the plane of maximum deformation $y = 0$ for three different values of the reduced activity E_2 , while keeping $E_1 = 10^{-1}$

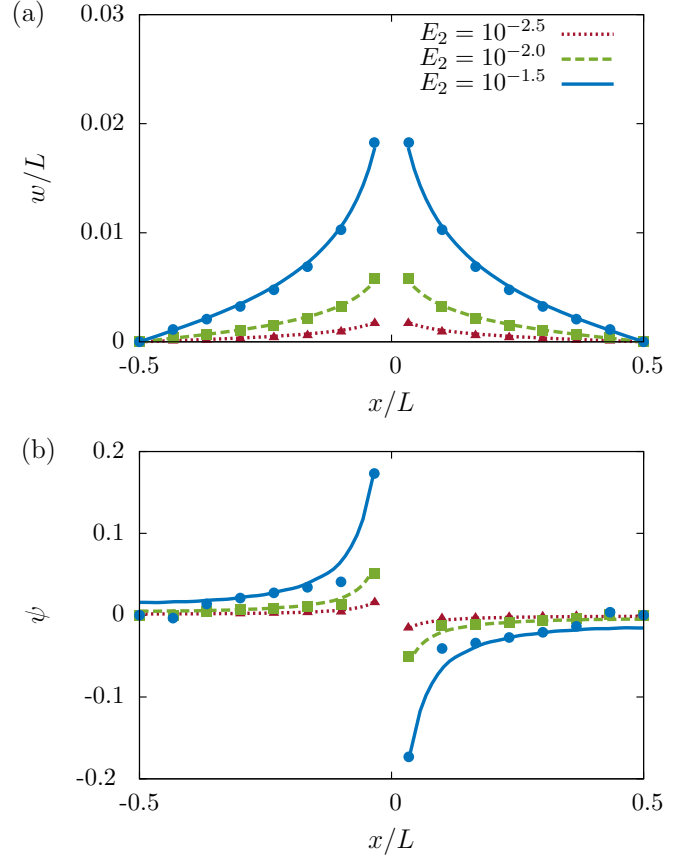


Figure 5. (Color online) Comparison between analytical predictions (solid lines) and full numerical solution of Eqs. (2) – (6) (symbols) in the steady-state of membrane trapping for various values of E_2 , while keeping $E_1 = 10^{-1}$. (a) Membrane normal displacement and (b) dipole orientation versus scaled distance x/L calculated in the plane of maximum deformation $y = 0$. Here, we consider a weakly-elastic membrane for which $\kappa = 1$. Thus, the dipolar and elastic interactions have essentially comparable effects on the overall membrane behavior.

and $\kappa = 1$. Symbols indicate the numerical solution of the full nonlinear problem given by Eqs. (2) – (6) and solid lines are the analytical predictions obtained from the solution of the continuum equations using finite Fourier transforms. Good agreement is found between the theory and simulations. The small discrepancy observed for ψ around the origin and near the membrane periphery is a drawback of the present analytical approach based on a perturbation technique. All in all, our predictive model requires no fitting parameters and thus can conveniently be applied to describe the steady-state membrane displacement and dipole orientation in the small-deformation regime considered here.

D. Transient dynamics

Having investigated the system behavior in the steady trapping limit, we next turn our attention to the transient

dynamics under the action of the force exerted by an active particle pushing against the membrane. To be able to make an analytical progress, we assume that $\delta \dot{z}_P \ll \mu_0 F$, such that F_0 is balanced by the steric interaction with the membrane, not by friction with the fluid. Accordingly, we set $\dot{z}_P = 0$ in Eq. (22) for $t > 0$.

By projecting Eq. (23) onto the x direction, it follows that ϕ necessarily vanishes. In this way, the projected equations of motion governing the temporal evolution of the normal displacement field w and orientation ψ read

$$\frac{w_{,t}}{A} = (k_{\parallel} + c) w_{,xx} + k_{\perp} w_{,yy} - c\psi_{,x} + hP_0 \delta(x, y), \quad (35a)$$

$$\frac{\psi_{,t}}{B} = 2c(w_{,x} - \psi). \quad (35b)$$

Using a similar solution procedure as for the steady dynamics that is based on Fourier transforms, we obtain

$$\frac{\hat{w}_{,t}}{A} = -(k_{\parallel} + c) H_p^2 \hat{w} - k_{\perp} H_q^2 \hat{w} - cH_p \hat{\psi} + hP_0, \quad (36a)$$

$$\frac{\hat{\psi}_{,t}}{B} = -2c(\hat{\psi} + H_p \hat{w}), \quad (36b)$$

where $\hat{\psi}$ denotes the Fourier coefficients of ψ , defined as

$$\hat{\psi}(p, q) = \int_{-\frac{L}{2}}^{\frac{L}{2}} \int_{-\frac{L}{2}}^{\frac{L}{2}} \psi(x, y) s_p(x) c_q(y) dx dy. \quad (37)$$

Applying Laplace transforms¹⁰⁷ to Eqs. (36) and solving for the unknown fields \hat{w} and $\hat{\psi}$, we readily obtain

$$\hat{w}(p, q) = \frac{A(s + 2cB)hP_0}{Q(s)}, \quad (38a)$$

$$\hat{\psi}(p, q) = -\frac{2cABH_p hP_0}{Q(s)}, \quad (38b)$$

with the denominator given by

$$Q(s) = s \left(s^2 + (((k_{\parallel} + c) H_p^2 + k_{\perp} H_q^2) A + 2cB) s + 2cAB(k_{\parallel} H_p^2 + k_{\perp} H_q^2) \right). \quad (39)$$

The expressions of the Fourier coefficients in the time domain follow forthwith by inverse Laplace transform as

$$\frac{\hat{w}}{\hat{w}_{\infty}} = 1 - e^{-\beta t} \left(\cosh(\tau t) + \frac{\tau^2 - \beta^2 + 2cB\beta}{2cB\tau} \sinh(\tau t) \right),$$

$$\frac{\hat{\psi}}{\hat{\psi}_{\infty}} = 1 - e^{-\beta t} \left(\cosh(\tau t) + \frac{\beta}{\tau} \sinh(\tau t) \right),$$

where \hat{w}_{∞} and $\hat{\psi}_{\infty}$ represent the steady normal displacement and orientation, respectively given by

$$\hat{w}_{\infty} = \frac{hP_0}{k_{\parallel} H_p^2 + k_{\perp} H_q^2}, \quad \hat{\psi}_{\infty} = -H_p \hat{w}_{\infty},$$

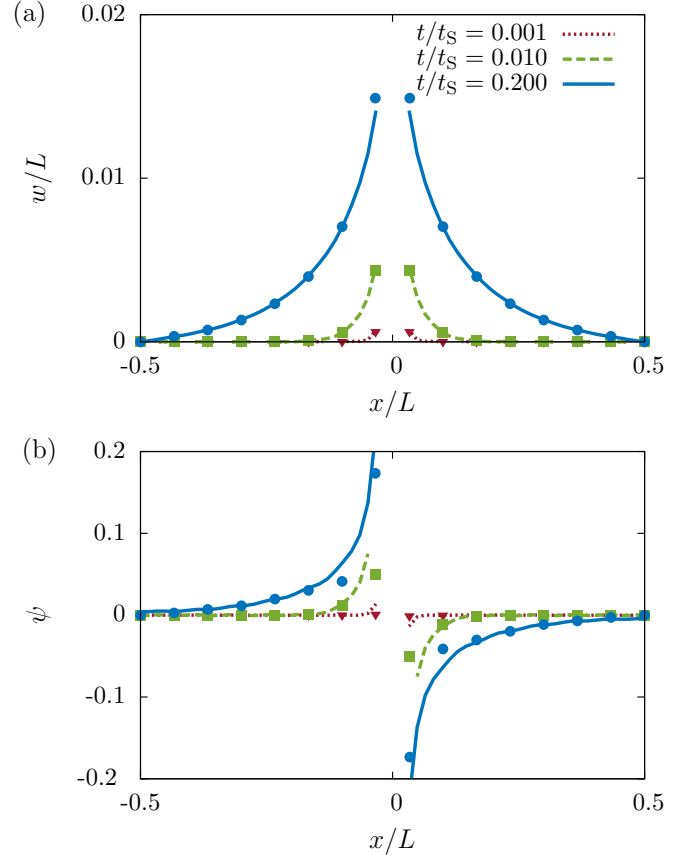


Figure 6. (Color online) Comparison between analytical predictions (solid lines) and full numerical simulations (symbols) for the transient behavior before the trapping state at various scaled times where, again, $t_S = \eta L^3 / \epsilon$ denotes the unit of simulation time. (a) Membrane normal displacement and (b) dipole orientation out of the plane of the undeformed membrane as functions of scaled distance x/L calculated in the plane $y = 0$. Here, we set $(E_1, E_2) = (10^{-1}, 10^{-1.5})$ and consider a weakly elastic membrane such that $\kappa = 1$.

and

$$\beta = \frac{1}{2} \left(((k_{\parallel} + c) H_p^2 + k_{\perp} H_q^2) A + 2cB \right), \quad (40a)$$

$$\tau = \left(\beta^2 - 2cAB(k_{\parallel} H_p^2 + k_{\perp} H_q^2) \right)^{1/2}, \quad (40b)$$

are inverse characteristic times, such that $0 < \tau < \beta$.

In Fig. 6, we present the transient evolution of (a) the membrane normal displacement and (b) the dipole orientation before reaching the steady-state at three scaled times, where $t_S = \eta L^3 / \epsilon$ denotes the simulation time. Here, curves are shown in the plane $y = 0$ using the membrane parameters $(E_1, E_2) = (10^{-1}, 10^{-1.5})$ and $\kappa = 1$. Although the analytical theory involves no fitting parameters, very good agreement is obtained between full numerical simulations (symbols) and analytical predictions (solid lines).

V. CONCLUSION

In the present work, we have discussed the interaction of an active particle with a minimal 2D membrane which could be realized, e.g., using synthetic particles of controlled interactions. We have identified three different scenarios, one corresponding to a permanent trapping of the particle by the membrane and the remaining two implying penetration of the particle through the membrane. The first type of penetration is characterized by a complete subsequent healing of the membrane which relaxes towards its equilibrium configuration once the particle has passed. In stark contrast, we have shown that much larger particles can create a hole in the membrane that is large enough to prevent such a self-healing dynamics, resulting in a permanently damaged membrane. This behavior is accompanied by the expulsion of membrane particles into isolated fragments. Our result suggests that if one were to effectively damage a synthetic vesicle, or perhaps a cancer cell membrane, one would need to use particles of a certain minimal size. Complementary to simulations, we here provide a detailed analytical theory allowing to predict the entire state diagram, the shape and the dynamics of the membrane. Our approach might be useful to predict transitions between trapping, penetration with and without self-healing in experiments.

ACKNOWLEDGMENTS

We thank Joachim Clement and Cornelia Monzel for stimulating discussions. The authors gratefully acknowledge support from the DFG (Deutsche Forschungsgemeinschaft) through the projects DA 2107/1-1, ME 3571/2-2, and LO 418/16-3.

REFERENCES

- ¹I. Budin and N. K. Devaraj, “Membrane assembly driven by a biomimetic coupling reaction,” *J. Am. Chem. Soc.* **134**, 751–753 (2011).
- ²Y. Osada and T. Nakagawa, *Membrane Science and Technology* (CRC Press, Boca Raton, Florida, 1992).
- ³G. Belfort, *Synthetic Membrane Process: Fundamentals and Water Applications* (Academic Press, Inc., Orlando, Florida, 2012).
- ⁴A. T. Brown and P. Cicuta, “Biological fluid interfaces and membranes,” in *The Oxford Handbook of Soft Condensed Matter* (2017).
- ⁵A. G. Fane, R. Wang, and M. X. Hu, “Synthetic membranes for water purification: status and future,” *Angew. Chem. Int. Ed.* **54**, 3368 (2015).
- ⁶I. Kocsis, M. Sorci, H. Vanselous, S. Murail, S. E. Sanders, E. Lic-sandru, Y.-M. Legrand, A. van der Lee, M. Baaden, P. B. Petersen, *et al.*, “Oriented chiral water wires in artificial transmembrane channels,” *Sci. Adv.* **4**, eaao5603 (2018).
- ⁷J. Vienken, M. Diamantoglou, W. Henne, and B. Nederlof, “Artificial dialysis membranes: from concept to large scale production,” *Am. J. Nephrol.* **19**, 355–362 (1999).
- ⁸H. Klinkmann and J. Vienken, “Membranes for dialysis,” *Nephrol. Dial. Transplant* **10**, 39 (1995).
- ⁹A. P. Davis, D. N. Sheppard, and B. D. Smith, “Development of synthetic membrane transporters for anions,” *Chem. Soc. Rev.* **36**, 348–357 (2007).
- ¹⁰Y.-R. Kim, S. Jung, H. Ryu, Y.-E. Yoo, S. M. Kim, and T.-J. Jeon, “Synthetic biomimetic membranes and their sensor applications,” *Sensors* **12**, 9530–9550 (2012).
- ¹¹I.-K. Jun and H. Hess, “A biomimetic, self-pumping membrane,” *Adv. Mater.* **22**, 4823–4825 (2010).
- ¹²R. Langer, “Drug delivery and targeting,” *Nature* **392**, 5–10 (1998).
- ¹³A. Verma, O. Uzun, Y. Hu, Y. Hu, H.-S. Han, N. Watson, S. Chen, D. J. Irvine, and F. Stellacci, “Surface-structure-regulated cell-membrane penetration by monolayer-protected nanoparticles,” *Nat. Mater.* **7**, 588 – 595 (2008).
- ¹⁴K. Yang and Y.-Q. Ma, “Computer simulation of the translocation of nanoparticles with different shapes across a lipid bilayer,” *Nat. Nanotech.* **5**, 579 (2010).
- ¹⁵J. Lin, H. Zhang, Z. Chen, and Y. Zheng, “Penetration of lipid membranes by gold nanoparticles: insights into cellular uptake, cytotoxicity, and their relationship,” *ACS Nano* **4**, 5421–5429 (2010).
- ¹⁶A. Verma and F. Stellacci, “Effect of surface properties on nanoparticle-cell interactions,” *Small* **6**, 12–21 (2010).
- ¹⁷A. E. Nel, L. Mädler, D. Velegol, T. Xia, E. M. Hoek, P. Somasundaran, F. Klaessig, V. Castranova, and M. Thompson, “Understanding biophysicochemical interactions at the nano-bio interface,” *Nat. Mater.* **8**, 543 (2009).
- ¹⁸T. Wang, J. Bai, X. Jiang, and G. U. Nienhaus, “Cellular uptake of nanoparticles by membrane penetration: a study combining confocal microscopy with FTIR spectroelectrochemistry,” *ACS Nano* **6**, 1251–1259 (2012).
- ¹⁹L. Shang, K. Nienhaus, and G. U. Nienhaus, “Engineered nanoparticles interacting with cells: size matters,” *J. Nanobiotechnology* **12**, 5 (2014).
- ²⁰C. Monzel, C. Vicario, J. Piehler, M. Coppey, and M. Dahan, “Magnetic control of cellular processes using biofunctional nanoparticles,” *Chem. Sci.* **8**, 7330–7338 (2017).
- ²¹D. Liße, C. Monzel, C. Vicario, J. Manzi, I. Maurin, M. Coppey, J. Piehler, and M. Dahan, “Engineered ferritin for magnetogenetic manipulation of proteins and organelles inside living cells,” *Adv. Mater.* **29**, 1700189 (2017).
- ²²E. K. Müller, C. Gräfe, F. Wiekhorst, C. Bergemann, A. Weidner, S. Dutz, and J. H. Clement, “Magnetic nanoparticles interact and pass an in vitro co-culture blood-placenta barrier model,” *Nanomaterials* **8**, 108 (2018).
- ²³B. D. Chithrani, A. A. Ghazani, and W. C. W. Chan, “Determining the size and shape dependence of gold nanoparticle uptake into mammalian cells,” *Nano Lett.* **6**, 662–668 (2006).
- ²⁴K. Yang and Y. Q. Ma, “Computer simulation of the translocation of nanoparticles with different shapes across a lipid bilayer,” *Nat. Nanotechnol.* **5**, 579–583 (2010).
- ²⁵T. Dos Santos, J. Varela, I. Lynch, A. Salvati, and K. A. Dawson, “Quantitative assessment of the comparative nanoparticle-uptake efficiency of a range of cell lines,” *Small* **7**, 3341–3349 (2011).
- ²⁶A. Parodi, N. Quattrocchi, A. L. Van De Ven, C. Chiappini, M. Evangelopoulos, J. O. Martinez, B. S. Brown, S. Z. Khaled, I. K. Yazdi, M. V. Enzo, *et al.*, “Synthetic nanoparticles functionalized with biomimetic leukocyte membranes possess cell-like functions,” *Nat. Nanotechnol.* **8**, 61 (2013).
- ²⁷A. Daddi-Moussa-Ider, A. Guckenberger, and S. Gekle, “Long-lived anomalous thermal diffusion induced by elastic cell membranes on nearby particles,” *Phys. Rev. E* **93**, 012612 (2016).
- ²⁸F. Jünger, F. Kohler, A. Meinel, T. Meyer, R. Nitschke, B. Erhard, and A. Rohrbach, “Measuring local viscosities near plasma membranes of living cells with photonic force microscopy,” *Biophys. J.* **109**, 869–882 (2015).
- ²⁹C. Gräfe, I. Slabu, F. Wiekhorst, C. Bergemann, F. von Eggeling, A. Hochhaus, L. Trahms, and J. Clement, “Magnetic particle spectroscopy allows precise quantification of nanoparticles after passage through human brain microvascular endothelial cells,” *Phys. Med. Biol.* **61**, 3986 (2016).

- ³⁰S. Ramaswamy and M. Rao, "The physics of active membranes," *C. R. Acad. Sci., Ser. IV-Phys.-Astrophys.* **2**, 817–839 (2001).
- ³¹Y. Z. Yoon, J. Kotar, A. T. Brown, and P. Cicutta, "Red blood cell dynamics: from spontaneous fluctuations to non-linear response," *Soft Matter* **7**, 2042–2051 (2011).
- ³²D. Lacoste and P. Bassereau, "An update on active membrane," *Liposomes, Lipid Bilayers and Model Membranes: From Basic Research to Application*, 271 (2014).
- ³³S. Mitragotri and J. Lahann, "Physical approaches to biomaterial design," *Nat. Mater.* **8**, 15 (2009).
- ³⁴Y. Li, X. Li, Z. Li, and H. Gao, "Surface-structure-regulated penetration of nanoparticles across a cell membrane," *Nanoscale* **4**, 3768–3775 (2012).
- ³⁵J. Wong-Ekkabut, S. Baoukina, W. Triampo, I.-M. Tang, D. P. Tieleman, and L. Monticelli, "Computer simulation study of fullerene translocation through lipid membranes," *Nat. Nanotech.* **3**, 363 (2008).
- ³⁶G. Junot, G. Briand, R. Ledesma-Alonso, and O. Dauchot, "Active versus passive hard disks against a membrane: mechanical pressure and instability," *Phys. Rev. Lett.* **119**, 028002 (2017).
- ³⁷U. M. B. Marconi, A. Sarracino, C. Maggi, and A. Puglisi, "Self-propulsion against a moving membrane: Enhanced accumulation and drag force," *Phys. Rev. E* **96**, 032601 (2017).
- ³⁸A. Costanzo, J. Elgeti, T. Auth, G. Gompper, and M. Ripoll, "Motility-sorting of self-propelled particles in microchannels," *EPL* **107**, 36003 (2014).
- ³⁹A. Daddi-Moussa-Ider, S. Goh, B. Liebchen, C. Hoell, A. J. Mathijssen, F. Guzmán-Lastra, C. Scholz, A. M. Menzel, and H. Löwen, "Membrane penetration and trapping of an active particle," *J. Chem. Phys.* **150**, 064906 (2019).
- ⁴⁰V. Froltsov, R. Blaak, C. Likos, and H. Löwen, "Crystal structures of two-dimensional magnetic colloids in tilted external magnetic fields," *Phys. Rev. E* **68**, 061406 (2003).
- ⁴¹E. Barry and Z. Dogic, "Entropy driven self-assembly of nonamphiphilic colloidal membranes," *Proc. Natl. Acad. Sci. U.S.A.* **107**, 10348–10353 (2010).
- ⁴²M. Ewerlin, D. Demirbas, F. Brüßing, O. Petravic, A. A. Ünal, S. Valencia, F. Kronast, and H. Zabel, "Magnetic dipole and higher pole interaction on a square lattice," *Phys. Rev. Lett.* **110**, 177209 (2013).
- ⁴³R. Messina, L. A. Khalil, and I. Stanković, "Self-assembly of magnetic balls: From chains to tubes," *Phys. Rev. E* **89**, 011202 (2014).
- ⁴⁴A. Kaiser, K. Popowa, and H. Löwen, "Active dipole clusters: from helical motion to fission," *Phys. Rev. E* **92**, 012301 (2015).
- ⁴⁵F. Guzmán-Lastra, A. Kaiser, and H. Löwen, "Fission and fusion scenarios for magnetic microswimmer clusters," *Nat. Commun.* **7**, 13519 (2016).
- ⁴⁶A. B. Yener and S. H. L. Klapp, "Self-assembly of three-dimensional ensembles of magnetic particles with laterally shifted dipoles," *Soft Matter* **12**, 2066–2075 (2016).
- ⁴⁷L. Spiteri and R. Messina, "Columnar aggregation of dipolar chains," *Europhys. Lett.* **120**, 36001 (2017).
- ⁴⁸R. Messina and I. Stanković, "Assembly of magnetic spheres in strong homogeneous magnetic field," *Physica A* **466**, 10 – 20 (2017).
- ⁴⁹S. D. Peroukidis and S. H. L. Klapp, "Orientational order and translational dynamics of magnetic particle assemblies in liquid crystals," *Soft Matter* **12**, 6841–6850 (2016).
- ⁵⁰F. Deisenbeck, H. Löwen, and E. C. Ögüz, "Ground state of dipolar hard spheres confined in channels," *Phys. Rev. E* **97**, 052608 (2018).
- ⁵¹J. García-Torres, C. Calero, F. Sagués, I. Pagonabarraga, and P. Tierno, "Magnetically tunable bidirectional locomotion of a self-assembled nanorod-sphere propeller," *Nat. Commun.* **9**, 1663 (2018).
- ⁵²E. C. Ögüz, A. Mijailović, and M. Schmiedeberg, "Self-assembly of complex structures in colloid-polymer mixtures," *Phys. Rev. E* **98**, 052601 (2018).
- ⁵³B. ten Hagen, S. van Teeffelen, and H. Löwen, "Brownian motion of a self-propelled particle," *J. Physics: Condens. Matter* **23**, 194119 (2011).
- ⁵⁴R. Wittkowski and H. Löwen, "Self-propelled brownian spinning top: dynamics of a biaxial swimmer at low reynolds numbers," *Phys. Rev. E* **85**, 021406 (2012).
- ⁵⁵A. Kaiser, H. Wensink, and H. Löwen, "How to capture active particles," *Phys. Rev. Lett.* **108**, 268307 (2012).
- ⁵⁶H. H. Wensink and H. Löwen, "Emergent states in dense systems of active rods: from swarming to turbulence," *J. Phys.: Condens. Matter* **24**, 464130 (2012).
- ⁵⁷F. Kümmel, B. ten Hagen, R. Wittkowski, I. Buttinoni, R. Eichhorn, G. Volpe, H. Löwen, and C. Bechinger, "Circular motion of asymmetric self-propelling particles," *Phys. Rev. Lett.* **110**, 198302 (2013).
- ⁵⁸B. Ten Hagen, F. Kümmel, R. Wittkowski, D. Takagi, H. Löwen, and C. Bechinger, "Gravitaxis of asymmetric self-propelled colloidal particles," *Nat. Commun.* **5**, 4829 (2014).
- ⁵⁹B. ten Hagen, R. Wittkowski, D. Takagi, F. Kümmel, C. Bechinger, and H. Löwen, "Can the self-propulsion of anisotropic microswimmers be described by using forces and torques?" *J. Phys. Condes. Matter* **27**, 194110 (2015).
- ⁶⁰T. Speck and R. L. Jack, "Ideal bulk pressure of active Brownian particles," *Phys. Rev. E* **93**, 062605 (2016).
- ⁶¹J. de Graaf, H. Menke, A. J. T. M. Mathijssen, M. Fabritius, C. Holm, and T. N. Shendruk, "Lattice-boltzmann hydrodynamics of anisotropic active matter," *J. Chem. Phys.* **144**, 134106 (2016).
- ⁶²B. Liebchen, D. Marenduzzo, and M. E. Cates, "Phoretic interactions generically induce dynamic clusters and wave patterns in active colloids," *Phys. Rev. Lett.* **118**, 268001 (2017).
- ⁶³C. Hoell, H. Löwen, and A. M. Menzel, "Dynamical density functional theory for circle swimmers," *New J. Phys.* **19**, 125004 (2017).
- ⁶⁴A. Daddi-Moussa-Ider and A. M. Menzel, "Dynamics of a simple model microswimmer in an anisotropic fluid: Implications for alignment behavior and active transport in a nematic liquid crystal," *Phys. Rev. Fluids* **3**, 094102 (2018).
- ⁶⁵E. Lauga and T. R. Powers, "The hydrodynamics of swimming microorganisms," *Rep. Prog. Phys.* **72**, 096601 (2009).
- ⁶⁶A. Zöttl and H. Stark, "Emergent behavior in active colloids," *J. Phys.: Condens. Matter* **28**, 253001 (2016).
- ⁶⁷E. Lauga, "Bacterial hydrodynamics," *Ann. Rev. Fluid Mech.* **48**, 105–130 (2016).
- ⁶⁸J. Elgeti, R. G. Winkler, and G. Gompper, "Physics of microswimmers – single particle motion and collective behavior: A review," *Rep. Prog. Phys.* **78**, 056601 (2015).
- ⁶⁹C. Bechinger, R. Di Leonardo, H. Löwen, C. Reichhardt, G. Volpe, and G. Volpe, "Active particles in complex and crowded environments," *Rev. Mod. Phys.* **88**, 045006 (2016).
- ⁷⁰P. Illien, R. Golestanian, and A. Sen, "Fuelled motion: phoretic motility and collective behaviour of active colloids," *Chem. Soc. Rev.* **46**, 5508–5518 (2017).
- ⁷¹W. Gao, X. Feng, A. Pei, C. R. Kane, R. Tam, C. Hennessy, and J. Wang, "Bioinspired helical microswimmers based on vascular plants," *Nano Lett.* **14**, 305–310 (2013).
- ⁷²W. Gao and J. Wang, "Synthetic micro/nanomotors in drug delivery," *Nanoscale* **6**, 10486–10494 (2014).
- ⁷³C. Scholz, M. Engel, and T. Pöschel, "Rotating robots move collectively and self-organize," *Nat. Commun.* **9**, 931 (2018).
- ⁷⁴C. Scholz, S. Jahanshahi, A. Ldov, and H. Löwen, "Inertial delay of self-propelled particles," *Nat. Commun.* **9**, 5156 (2018).
- ⁷⁵W. R. Adey, "Models of membranes of cerebral cells as substrates for information storage," *Biosystems* **8**, 163–178 (1977).
- ⁷⁶J. Jiang, K. B. Eisenthal, and R. Yuste, "Second harmonic generation in neurons: electro-optic mechanism of membrane potential sensitivity," *Biophys. J.* **93**, L26–L28 (2007).
- ⁷⁷A. F. Demirörs, J. C. Stiefelwagen, T. Vissers, F. Smallenburg, M. Dijkstra, A. Imhof, and A. van Blaaderen, "Long-ranged oppositely charged interactions for designing new types of colloidal clusters," *Phys. Rev. X* **5**, 021012 (2015).
- ⁷⁸N. S. Gov, "Active elastic network: cytoskeleton of the red blood cell," *Phys. Rev. E* **75**, 011921 (2007).

- ⁷⁹Z. Peng, X. Li, I. V. Pivkin, M. Dao, G. E. Karniadakis, and S. Suresh, "Lipid bilayer and cytoskeletal interactions in a red blood cell," *Proc. Natl. Acad. Sci. U.S.A.* **110**, 13356–13361 (2013).
- ⁸⁰C. O. Mejean, A. W. Schaefer, K. B. Buck, H. Kress, A. Shundrovsky, J. W. Merrill, E. R. Dufresne, and P. Forscher, "Elastic coupling of nascent apcam adhesions to flowing actin networks," *PLoS One* **8**, e73389 (2013).
- ⁸¹J. D. Weeks, D. Chandler, and H. C. Andersen, "Role of repulsive forces in determining the equilibrium structure of simple liquids," *J. Chem. Phys.* **54**, 5237–5247 (1971).
- ⁸²S. Babel, H. Löwen, and A. M. Menzel, "Dynamics of a linear magnetic microswimmer molecule," *Europhys. Lett.* **113**, 58003 (2016).
- ⁸³J. Happel and H. Brenner, *Low Reynolds Number Hydrodynamics: with Special Applications to Particulate Media* (Springer Science & Business Media, The Netherlands, 2012).
- ⁸⁴S. Kim and S. J. Karrila, *Microhydrodynamics: Principles and Selected Applications* (Courier Corporation, 2013).
- ⁸⁵J. W. Swan and J. F. Brady, "Simulation of hydrodynamically interacting particles near a no-slip boundary," *Phys. Fluids* **19**, 113306 (2007).
- ⁸⁶J. W. Swan and J. F. Brady, "Particle motion between parallel walls: Hydrodynamics and simulation," *Phys. Fluids* **22**, 103301 (2010).
- ⁸⁷F. Balboa-Usabiaga, B. Kallemov, B. Delmotte, A. Bhalla, B. Griffith, and A. Donev, "Hydrodynamics of suspensions of passive and active rigid particles: a rigid multiblob approach," *Comm. App. Math. Com. Sc.* **11**, 217–296 (2017).
- ⁸⁸M. Driscoll and B. Delmotte, "Leveraging collective effects in externally driven colloidal suspensions: Experiments and simulations," *Curr. Opin. Colloid Interface Sci.* (2018).
- ⁸⁹W. H. Press, *The Art of Scientific Computing* (Cambridge University Press, 1992).
- ⁹⁰D. Vella, E. du Pontavice, C. L. Hall, and A. Goriely, "The magneto-elastica: from self-buckling to self-assembly," *Proc. Royal Soc. A* **470** (2014).
- ⁹¹C. L. Hall, D. Vella, and A. Goriely, "The mechanics of a chain or ring of spherical magnets," *SIAM J. Appl. Math.* **73**, 2029–2054 (2013).
- ⁹²W. Jiang, B. Y. Kim, J. T. Rutka, and W. C. Chan, "Nanoparticle-mediated cellular response is size-dependent," *Nat. Nanotechnol.* **3**, 145 (2008).
- ⁹³P. O. Andersson, C. Lejon, B. Ekstrand-Hammarström, C. Akfur, L. Ahlinder, A. Bucht, and L. Österlund, "Polymorph-and size-dependent uptake and toxicity of tio2 nanoparticles in living lung epithelial cells," *Small* **7**, 514–523 (2011).
- ⁹⁴E. Oh, J. B. Delehanty, K. E. Sapsford, K. Susumu, R. Goswami, J. B. Blanco-Canosa, P. E. Dawson, J. Granek, M. Shoff, Q. Zhang, *et al.*, "Cellular uptake and fate of pegylated gold nanoparticles is dependent on both cell-penetration peptides and particle size," *ACS Nano* **5**, 6434–6448 (2011).
- ⁹⁵W. Huang, C. B. Chang, and H. J. Sung, "Three-dimensional simulation of elastic capsules in shear flow by the penalty immersed boundary method," *Journal of Computational Physics* **231**, 3340–3364 (2012).
- ⁹⁶A. Elbakry, E.-C. Wurster, A. Zaky, R. Liebl, E. Schindler, P. Bauer-Kreisel, T. Blunk, R. Rachel, A. Goepferich, and M. Breunig, "Layer-by-layer coated gold nanoparticles: Size-dependent delivery of DNA into cells," *Small* **8**, 3847–3856 (2012).
- ⁹⁷S. Goh, A. M. Menzel, and H. Löwen, "Dynamics in a one-dimensional ferrogel model: relaxation, pairing, shock-wave propagation," *Phys. Chem. Chem. Phys.* **20**, 15037–15051 (2018).
- ⁹⁸A. M. Menzel, "Mesoscopic characterization of magnetoelastic hybrid materials: magnetic gels and elastomers, their particle-scale description, and scale-bridging links," *Arch. Appl. Mech.* **89**, 17–45 (2019).
- ⁹⁹S. P. Timoshenko and S. Woinowsky-Krieger, *Theory of Plates and Shells*, Vol. 2 (McGraw-hill, New York, 1959).
- ¹⁰⁰M. H. Sadd, *Elasticity: Theory, Applications, and Numerics* (Academic Press, Cambridge, Massachusetts, 2009).
- ¹⁰¹A. Daddi-Moussa-Ider, A. Guckenberger, and S. Gekle, "Particle mobility between two planar elastic membranes: Brownian motion and membrane deformation," *Phys. Fluids* **28**, 071903 (2016).
- ¹⁰²A. Daddi-Moussa-Ider, B. Rallabandi, S. Gekle, and H. A. Stone, "Reciprocal theorem for the prediction of the normal force induced on a particle translating parallel to an elastic membrane," *Phys. Rev. Fluids* **3**, 084101 (2018).
- ¹⁰³A. Daddi-Moussa-Ider and S. Gekle, "Brownian motion near an elastic cell membrane: A theoretical study," *Eur. Phys. J. E* **41**, 19 (2018).
- ¹⁰⁴A. Daddi-Moussa-Ider, M. Lisicki, S. Gekle, A. M. Menzel, and H. Löwen, "Hydrodynamic coupling and rotational mobilities near planar elastic membranes," *J. Chem. Phys.* **149**, 014901 (2018).
- ¹⁰⁵P. Rosenau, "Hamiltonian dynamics of dense chains and lattices: or how to correct the continuum," *Phys. Lett. A* **311**, 39–52 (2003).
- ¹⁰⁶R. Bracewell, *The Fourier Transform and Its Applications* (McGraw-Hill, Pennsylvania, 1999).
- ¹⁰⁷D. V. Widder, *Laplace Transform (PMS-6)* (Princeton University Press, New Jersey, 2015).